Substantiating the Influence of Pore Surface Functionalities on the Stability of Grubbs Catalyst in Mesoporous SBA-15 Silica

Hélène Staub, [a,b,c] *Rémy Guillet-Nicolas,* [a,b] *Nicolas Even,*[a] *Laure Kayser,*[a] *Freddy Kleitz** [a,b] *and Frédéric-Georges Fontaine** [a,c]

[a] H. Staub, R. Guillet-Nicolas, N. Even, L. Kayser, Prof. F. Kleitz, Prof. F.-G. Fontaine

Department of Chemistry, Université Laval, 1045 Avenue de la Médecine, Québec (Qc), G1V 0A6 (Canada)

[b] Centre de recherche sur les matériaux avancés (CERMA), Université Laval,

[c] Centre de recherche sur la propriété des interfaces et de la catalyse (CERPIC), Université Laval.

E-mails: frederic.fontaine@chm.ulaval.ca, freddy.kleitz@chm.ulaval.ca

This is the peer reviewed version of the following article: [Substantiating the Influence of Pore Surface Functionalities on the Stability of Grubbs Catalyst in Mesoporous SBA-15 Silica, Chem. Eur. J. 2011, 17, 4254 – 4265], which has been published in final form at [10.1002/chem.201002740].

Abstract: The influence of pore surface functionalities in mesoporous SBA-15 silica on the stability of a model olefin metathesis catalyst, namely Grubbs I, is substantiated. In particular, it is demonstrated that the nature of the interaction between the ruthenium complex and the surface is strongly depending on the presence of surface silanols. For this study, differently functionalized mesoporous SBA-15 silica materials were synthesized according to standard procedures and, subsequently, the Grubbs I catalyst was incorporated into these different host materials. All of the materials were thoroughly characterized by elemental analyses, nitrogen physisorption at -196 °C, thermogravimetric analyses, solid state NMR spectroscopy, and infrared spectroscopy (ATR-IR). By such in-depth characterization of the materials, it became possible to achieve models for the surface/catalyst interactions as a function of surface functionalities in SBA-15, e.g. in the case of purely siliceous silanol-rich SBA-15, octenyl-silane modified SBA-15, and silylated equivalents. It was evidenced that large portions of the chemisorbed species that are detected spectroscopically arise from interactions between the tricyclohexylphosphine and the surface silanols. A catalytic study using diethyldiallylmalonate in presence of the various functionalized silicas shows that the presence of surface silanols significantly decreases the longevity of the ring-closing metathesis catalyst, whereas the passivation of the surface by trimethylsilyl groups slows down the catalysis rate, but does not affect significantly the lifetime of the catalyst. This contribution thus provides new insights into the functionalization of SBA-15 materials and the role of surface interactions for the grafting of organometallic complexes.

Keywords: mesoporous silica, SBA-15, heterogeneous catalysis, surface functionalization, Grubbs catalyst, olefin metathesis, phosphine

Introduction

Olefin metathesis has been discovered in the 1950's by researchers at Dupont,[1] but only in the past fifteen years has its applications in synthesis spurred widely, owing to the commercialization of durable catalysts prepared initially by Schrock[2] and Grubbs,[3] which culminated by the award of the Nobel prize in 2005. The first-generation Grubbs' catalyst, $(PCy_3)_2Ru(Cl)_2=C(H)(Ph)$, remains one of the most abundantly used homogeneous species for the metathesis reaction, although more durable and more active generations of catalysts have been produced since.[4] However, there are some stringent requirements that limit the use of metathesis catalysts in industry, especially in the pharmaceutical industry. One of the requirements is the removal of trace transition metals from the products. In order to do so, two main strategies are implemented: the immobilization of the catalysts on solid supports and scavenging of residual catalysts. In both case, several materials have been applied as supports or scavengers,[5] and porous silica has proved to be one of the most appropriate. To date, a large variety of supported catalytic systems and metal scavengers have thus been described in the literature, based on a wide range of silica supports.[6]

Whereas the first report of the immobilization of Grubbs' catalyst was on a polystyrene-divinylbenzene copolymer through phosphine exchange, as demonstrated by Grubbs in 1995,[7] it was not until 2001 that the incorporation of this ubiquitous catalyst on mesoporous silica was carried out.[8] Condensation of a triethoxysilyl-functionalized diphenyl and dicyclohexylphosphine ruthenium carbene complex on MCM-41 silica allowed the formation of a material showing good catalytic activity in ring-closing metathesis (RCM) and ring-opening metathesis polymerization (ROMP), albeit inferior to the homogeneous system. Since these pioneer findings, several generations of Grubbs' catalyst were supported on silica by grafting ancillary ligands onto the surface.[9] However, most catalysts have a low activity compared to their homogeneous analogues

and substantial leaching of the ruthenium is observed.

One major limitation with the grafting of Grubbs' catalyst on a solid support is the diffusion of the catalyst to the liquid phase. Mechanistic studies have shown that one key step in the activation of the first-generation Grubbs' catalyst is the loss of one phosphine ligand.[10] However, on a mesoporous solid support, the catalyst will have to overcome interactions with the surface (functionalized or not) as well as with other grafted substituents in order to obtain the desired catalytic activity. In order for the catalyst to keep its optimal activity, proper understanding of the grafting properties must be acquired. A recent report by Polarz[11] allowed to gain several useful insights into the interactions between Grubbs' catalyst and mesoporous MCM-41-type material. In this study, the authors thoroughly characterized the ruthenium side-products in the liquid-phase, thus obtaining circumstantial evidence of interactions between the catalyst and silica. In the present contribution, we wish to supplement the above findings by focusing specifically on the solid-state characterization of differently functionalized-SBA-15 silica materials and their interactions with the Grubbs I catalyst and the liberated phosphine species. These findings will not only provide valuable insights into the reactivity of silica with Grubbs' type catalysts and the influence of surface functional groups in such a system, but will also be of use to understand most phosphine-containing catalytic systems.

RESULTS

Material synthesis, porosity, and thermal behavior. For this study, four functional mesoporous materials were selected as host to Grubbs I catalyst. In addition to the pristine SBA-15 silica, three organo-functionalized materials were also prepared. SBA-15 was synthesized according to the standard

procedure developed by Choi et al. in 2003.[12] Surface functionalization was performed by post-synthesis grafting of organosilanes in dry toluene under reflux conditions (See Experimental Section). First, SBA-15/C_8 was synthesized by tethering 3.25 equivalents of 1-octenyl-7-trichlorosilane onto the surface of SBA-15, which exhibited a concentration of surface silanols of 1.29 mmol/g, as evaluated by titration following a published procedure.[13] The octenyl group offers an hydrophobic environment as well as a long alkenyl chain that can undergo olefin metathesis with neighboring functionalities, helping to characterize the presence of Grubbs' catalyst within the pores. The addition of an excess of hexamethyldisilazane (HMDS) to the pure SBA-15 silica and the above hybrid SBA-15/C_8 afforded two additional functionalized materials which are denoted SBA-15* and SBA-15*/C_8, respectively (see Scheme 1). The addition of the trimethylsilyl moieties from HMDS will passivate the pore surface of the materials by binding to the remaining surface silanols, which will help discriminating the role of the silanols in the sorption and diffusion of the molecular catalyst.

All the four support materials exhibit similar nitrogen sorption properties, showing typical type IV isotherms characteristic of highly ordered materials with large mesopores (Figure 1).[14,15] In all cases, the contribution of external surface area to the total porosity of the materials is obviously very small and will thus be neglected. The physicochemical parameters derived from nitrogen physisorption for the parent SBA-15 and the differently functionalized materials are grouped in Table 1. As expected, the introduction of organic moieties within the pores of SBA-15 results in decreased adsorption capacity, which is reflected by significantly lower BET specific surface areas and reduced pore volumes as compared to the parent SBA-15. It is furthermore observed that the introduction of C8 alkyl chains in SBA-15 leads to a substantial decrease of the mesopore size of the material from 8.5 nm to 7.6 nm (NLDFT pore sizes). Silanol (SiOH) passivation using HMDS results in the case of the pristine SBA-15 sample in a noticeable pore size reduction of about 0.5-0.6 nm (from NLDFT or BJH analyses). Such a

decrease in pore size is fairly consistent with previous observations concerning TMS insertion in MCM-41 or SBA-15 materials [16,17]. Interestingly, the passivation of SBA-15/C_8 using HMDS also induces a further decrease in pore size. Clearly, SBA-15*/C_8 shows the lowest adsorption capacity of all samples, with a BET of 370 $m^2\ g^{-1}$ and pore volume of 0.59 $cm^3\ g^{-1}$, and the smallest pore size (7.05 nm). However, in no case is pore blocking observed and the open cylindrical pore geometry is maintained, with well-defined H1-type hysteresis loops (e.g. pore size values obtained from the desorption branch are not smaller than those obtained from adsorption branch).[18] Moreover, from the cumulative pore volume plots (Figure 1b), one can see that the parent SBA-15 silica prepared under our conditions exhibits substantial amount of complementary intra-wall porosity (volume estimated for pores < 6 nm), in agreement with previous reports.[12,18-20] For this SBA-15 sample, the intra-wall pore volume reaches 0.2 $cm^3\ g^{-1}$ as estimated from the NLDFT cumulative pore volume of pores smaller than 6 nm. However, upon silanol passivation using HMDS in toluene, e.g. SBA-15*, this intra-wall pore volume is noticeably reduced. On the other hand, materials modified with C8 alkyl chains do not exhibit any apparent intra-wall pore volume remaining. Therefore, a possible contribution of intra-wall micropores/small mesopores on the reactivity towards the Grubbs catalyst can be neglected for these two latter materials.

The thermogravimetric analysis (TGA) curves obtained for the different organic-containing mesoporous materials, e.g. SBA-15/C_8, SBA-15*, and SBA-15*/C_8, are depicted in Figure 2. The corresponding weight losses (%) and elemental analysis (EA) results are compiled in Table 2 and Table 3, respectively. The presence of organic moieties in SBA-15/C_8 can be judged from the 15% weight loss starting at about 210 ^oC and completed at about 500 ^oC, and by the presence of carbon and hydrogen by EA (10.5% and 2.8%, respectively). After HMDS-silanol passivation of the above material, one does observe a reproducible decrease in the overall weight loss from 15% to 14%, although elemental analyses suggest

higher quantities of occluded organics (Table 2). Furthermore, thermal analysis shows that the organics remain stable up to 300 ºC, which is more than 90 ºC above that of SBA-15/C_8, indicating that the capping of the residual silanols must affect the degradation profile. Indeed, Zaitsev and co-workers have demonstrated that the absence of silanol moieties on the surface in silica materials, such as expected for SBA-15*/C_8, could help to prevent degradation of surface organic layers up to temperatures as high as 700 ºC.[21] This effect, together with a much lower amount of H_2O evolved from limited residual silanol condensation, may account for this observation. The weight loss associated with the combustion of the trimethylsilyl (TMS) groups on the surface is less than 3% for the TMS-protected SBA-15* and occurs at temperatures above 400-420 ºC (the DTA peak is centred at 450 °C). In comparison, it was demonstrated that for fully TMS-protected MCM-41 the weight loss of the material is very small under 450 ºC and that it corresponds to irreversible water loss.[22] The differential thermal analysis (DTA) profiles also support the TGA conclusions (as illustrated on Figure 3). The combustion process for SBA-15/C_8 occurs at lower temperature than the one observed for the SBA-15*/C_8 material, once more suggesting that the protection of the surface could play a role in regulating the combustion process.

For all of the materials, the catalyst grafting procedure was performed by dispersing the different powders (200 or 500 mg) in a 4.8 mM solution of the Grubbs' catalyst in toluene for a period of 2 hours at room temperature. The resulting solids were then filtered, washed with methylene chloride using a Soxhlet extractor,[‡] yielding the materials designated as SBA-15-Ru, SBA-15/C_8-Ru, SBA-15*-Ru, and SBA-15*/C_8-Ru, from the different starting materials, respectively. From the TG analyses, it can be seen that the amount of organic material present in the solids after addition of the Grubbs catalyst has increased for both SBA-15-Ru and SBA-15/C_8-Ru samples, with total weight losses of 5 wt% (+ 2%) and 23 wt% (+7%), respectively (Figure 2). In both materials, a significant amount of Ru and P could be detected by elemental analyses which suggest insertion of the phosphine ruthenium complex on the

silica surface (Table 2), in agreement with the observations made by Polarz et al.[11] Differently, in the case of the TMS-protected material, SBA-15*/C_8-Ru, the weight loss is lower than that of SBA-15*/C_8, consistent with a lower organic content from elemental analyses (12.31% C and 2.33% H). This may be rationalized by the loss of C_2H_4 resulting from the RCM of the octenyl moieties (as illustrated in Scheme 2), as further demonstrated below by spectroscopic methods. In this case, the very low content of both Ru and P also would be in line with a low incorporation of Ru species inside the pores. The DTA profile of the SBA-15*/C_8-Ru material is also very similar to that of Grubbs' catalyst, which would suggest the residual Ru and P arise from inclusion and trapping of ruthenium complexes within the pores following the metathesis reaction of the octenyl moieties (Figure 4). A small additional weight loss is observed for SBA-15*-Ru compared to SBA-15-Ru (+1.5%), which can be associated to an exothermic effect occurring at 350 °C according to the DTA analysis, but this later effect is in a much smaller scale than observed for SBA-15-Ru and could again be associated with a small amount of ruthenium complexes trapped within the pores. In addition, for the SBA-15/C_8-Ru material, three major effects can be observed in the differential thermal analysis (DTA; Figure 3). The first one at 290 °C is reminiscent of the profile for the passivated materials, i.e. SBA-15*/C_8 and SBA-15*/C_8-Ru, thus suggesting the thermodesorption/decomposition of the grafted organic moieties. A second process occurs at 350 ^oC that is also present for the SBA-15-Ru material, suggesting that upon the addition of Grubbs' catalyst on the material, some residual organic moieties remain bound to the surface and interacting with silanols, since the same process is not observed in SBA-15*/C_8-Ru and very weak in SBA-15*-Ru. The third one, at 380 ^oC is very close to what has been observed for the degradation of a sample of the molecular Grubbs' catalyst suggesting that some grafted ruthenium species are responsible for it (Figure 4).

Nitrogen physisorption isotherms were also collected for the different supports after reaction with the Grubbs I catalyst (See Figures S1 in supporting information). When comparing the different isotherms,

one can observe a reduced adsorption capacity after reaction with the Grubb's catalyst for all samples but SBA-15*/C_8, which is consistent with the insertion of entities in the pores. [19,20] However, the effect of the ruthenium catalyst appears to be function of the surface modification which was applied. In absence of C8 alkyl chain modification, the well-defined hysteresis loops do not seem to be much affected by the presence of Ru species. No variation in pore size is visible, only volumes adsorbed are affected. In particular, the reaction with the Grubbs catalyst seems to result in decreased intra-wall porosity for SBA-15-Ru, as deduced from the NLDFT cumulative pore volumes (Figure S2), suggesting in that case that some of the catalyst is located in the complementary pores. In contrast, materials containing C8 chains show interesting additional features. SBA-15/C_8-Ru reveals not only changes in total pore volume but also in the capillary condensation and hysteresis behavior with a slightly smaller mesopore size (as clearly seen from the difference in the PSDs shown in Figure S3), which can originate from the space required for additional molecules immobilized in the mesopores or substantial modification of surface properties.[20] In the case of SBA-15*/C_8-Ru a slight increase in adsorption capacity is observed which is in line with the lower mass losses measured in TGA for this sample (12% *vs* 14% for SBA-15*/C_8), and thus consistent with removal of some organic chains and the absence of significant entrapment of ruthenium and phosphine species.

Spectroscopic characterization of the functionalized mesoporous materials. The organo-functionalized host materials and the Ru-modified samples were further characterized using solid state NMR spectroscopy to achieve additional insights into the nature of the surface-organometallic species. The CP/MAS ^{13}C NMR spectrum confirms the presence of the octenyl substituents in the SBA-15/C_8 sample, with the vinylic signals clearly visible at 119 and 147 ppm (Figure 5a). In the case of the SBA-15*/C_8, the presence of the TMS moieties is evidenced from the resonance at 0 ppm, which is also the single resonance present in SBA-15* (Figure 6a), as expected. Upon the addition of the Grubbs' catalyst, it can

be observed that the octenyl substituents in both olefin-containing materials, *i.e.* SBA-15*/C_8-Ru and SBA-15/C_8-Ru, have undergone olefin metathesis since the two original resonances have disappeared and a new one for the vinylic moieties can be observed at 133 ppm (Figures 5b and 6b), which is typical for an internal alkene. Although no organic moiety is originally present in the SBA-15 prior to the addition of Grubbs' catalyst, a single resonance can be observed at 27 ppm for SBA-15-Ru, which corresponds to the cyclohexyl moieties of PCy_3 (Figure 7a). In both SBA-15* and SBA-15*-Ru, no organic content other that TMS moieties is observed (Figure 7b-c).

In Figure 8a, the ^{31}P MAS NMR spectrum of SBA-15-Ru shows two distinct resonances at 56.1 and 30.5 ppm, in a 6:1 ratio, whereas the ratio for SBA-15/C_8-Ru is inverted (1:10; Figure 8b), but with two additional signals overlapping on the resonance at 30.5 ppm. In the case of SBA-15*/C_8-Ru (Figure 8c) and SBA-15*-Ru no signals were observed. To gain more information on the nature of the phosphorous species bound to silica, series of additional experiments were carried out. The direct addition of $OPCy_3$ on SBA-15 (SBA-15/$OPCy_3$) yielded only a single P species at 56.1 ppm (Figure 9b), thus suggesting that the downfield signal observed in the spectra of the grafted species corresponds to the sorption of oxidized phosphine on the surface. The addition of pure PCy_3 on SBA-15 (SBA-15/PCy_3) also exhibits a major resonance at 56.1 ppm, suggesting that the surface silanols participate in the oxidation of the phosphine, presumably during the Soxhlet treatment (Scheme 3a and Figure 9a). However, an additional P species is also present at 30.5 ppm. Hu et al. previously attributed the species at 30.5 ppm to the tricyclohexylphosphonium group interacting with silica, therefore signifying that the Lewis base can abstract a proton from the surface silanols to generate ion pairs, as illustrated in Scheme 3b.[23] However, the results of TG and elemental analyses (Tables 2 and 3) both imply that the sorption of the phosphine oxide is significantly more important than that of the phosphine. Indeed, it can be observed that the organic content (%C 6.62, %H 1.67, %P 0.97) and the weight loss (9.0%) in SBA-15/$OPCy_3$ are both

higher than those of SBA-15/PCy_3, which have respectively the values %C 4.30, %H 1.29, %P 0.26, and 5.5%. The addition of tricyclohexylphosphine to SBA-15/C_8 (SBA-15/C_8/PCy_3) also gives the same resonances at 56.1 and 30.5 ppm, however this time with a 1 : 20 ratio. Thus, it seems plausible that the presence of organic moieties on the surface could limit the oxidation process in favor of the formation of the phosphonium ion pairs. Therefore, the results suggest that most of the species observed in the ^{31}P NMR spectra arise from the interaction of free phosphine with silica. Although the octenyl chains renders difficult a comparison of the %C and %H, it can be observed that the phosphorous content in SBA-15/C_8/PCy_3 (0.81%) is larger than that in in SBA-15/PCy_3 (0.26%), which would imply that the presence of organic moieties helps retaining the phosphorous species inside the pores. Furthermore, the shoulders observed for the resonance at 30.5 ppm for SBA-15/C_8-Ru are probably attributed to phosphine ruthenium complexes, as also discussed by Polarz and co-workers.[11]

Attenuated total reflection infrared spectroscopy (ATR-IR) was used to analyze the surface of the materials. All materials, except for SBA-15, have the frequencies attributed to aliphatic C-H elongations of bound organic moieties, appearing at around 2920, 2850, and 1450 cm^{-1} (See Figure 10 and Figure S4) . For the TMS grafted materials, the presence of the Si-CH_3 elongations is also substantiated by the presence of signals at 2960 cm^{-1} (Figure 10) and 841 cm^{-1} (not shown). In both SBA-15/C_8 and SBA-15*/C_8, a sharp signal at 1641 cm^{-1} is observed which could be attributed to the alkene moiety, which is then no longer present in the materials after exposure to the Grubbs' catalyst (Figure S4). Instead, a broad band appears here above 1600 cm^{-1} after insertion of the Ru-species in these samples, and it is especially pronounced in the case of SBA-15/C_8-Ru. This signal may be assigned to the contribution of adsorbed molecular water (bending mode), more likely to be present in more hydrophilic samples. It may be speculated that the incorporated Ru-species might thus provide in these cases some hydrophilic adsorption sites. Note that such broad signal corresponding to adsorbed water is also clearly observed in

the case of pure SBA-15 silica and the SBA-15-Ru counterpart (Figure S4). Moreover, both SBA-15/C8 and SBA-15*/C_8 samples exhibit one additional signal centered around 3100 cm^{-1} which may be ascribed to olefinic C-H stretching (see Figure 10). The reaction of these supports with the Grubbs I catalyst results in the disappearance of this particular signal and the occurrence of two new vibrations, particularly visible for SBA-15*/C_8, in agreement with the possibility of ring-closing metathesis.

A very interesting feature of the ATR-IR spectra is the O-H stretching mode region (Figure 10). Two broad peaks centered at 3400 cm^{-1} and 3650 cm^{-1} are present for the surface -OH groups which are involved in hydrogen bonding with the immediate neighbors. Physisorbed molecular water may here also contribute to the signal at 3400 cm^{-1} (stretching mode of adsorbed H_2O) in correlation with the broad band above 1600 cm^{-1} discussed above. There is also a sharp peak at 3740 cm^{-1} corresponding to "free" silanol groups, not involved in hydrogen bonding. The materials having been functionalized, either or both, with the octenyl chain and the TMS group do not exhibit free silanols, as suggested by the absence of the vibration at 3740 cm^{-1} , which, in contrast, appeared both in SBA-15 and SBA-15-Ru. Although the absolute absorptivity in ATR-IR spectroscopy is not quantitative, we can observe that the ratio of the signals at 3400 and 3650 cm^{-1} is similar when comparing each SBA-15 material and its ruthenium-containing equivalent, with the exception of the SBA-15/C_8 and SBA-15/C_8-Ru spectra, where the 3400 cm^{-1} signal is much more intense after the addition of the Grubbs catalyst. The latter result suggests that surface modification after the addition of the Grubbs catalyst is more important in this sample than in the other three samples, which is in line with what is observed in the sorption, in the ^{31}P NMR spectra where the presence of numerous chemisorbed species is evident, and in the catalytic results, as demonstrated in the next section.

Catalytic metathesis experiments. Catalytic ring-closing metathesis experiments were carried out with the Grubbs' first generation catalyst and diethyldiallylmalonate as a model substrate, in order to

determine the influence of the different supports on the catalytic efficiency (Scheme 4). First, monitoring of the reaction of a 0.83 mM solution of Grubbs' catalyst in toluene with 80 equivalents of the test substrate in absence of any material showed a fine rate profile and showed that the reaction was going to completion after a little bit more than 200 minutes (Figure 11a). The addition of another 80 equivalents of diethyldiallylmalonate 300 minutes after the first addition does show that the catalyst is still active, but that the rate is somewhat slower (Figure 11b). Subsequently, in a series of comparative experiments, the various materials studied (*i.e.* SBA-15, SBA-15*, SBA-15/C_8, and SBA-15*/C_8) were added to the solution of the Grubbs' catalyst 10 minutes prior to addition of the substrate. The first observation was that the catalysis rate in presence of purely siliceous SBA-15 is relatively unaffected in the first catalytic run as compared to the homogeneous solution (Figure 11a). On the other hand, the addition of either SBA-15/C_8 or SBA-15*/C_8 materials reduced significantly the reaction rate. In the presence of SBA-15/C_8, the reaction leveled off at 40% conversion after 40 minutes, whereas in the reaction with SBA-15*/C_8, the conversion after 200 minutes reached more than 80%. In the case of SBA-15*, the conversion is slightly lower than in the homogeneous system or with SBA-15, but the conversion after 200 minutes is ultimately very similar. These results indicate that in presence of a hydrophobic coating (either an octenyl moiety or HMDS passivation), the transfer of the Grubbs' catalyst within the pores of the materials is enhanced, as confirmed by the ring-closing metathesis of the octenyl substituents in the SBA15/C_8-Ru and SBA15*/C_8-Ru materials, thus reducing the catalytic activity in solution. However, we observed that if the mesopore surface is passivated by HMDS, *i.e.* no silanols are present on the surface of the material; the Grubbs catalyst remains active and can diffuse out of pores to the solution medium. Moreover, it is well known that the active catalyst in Grubbs' mediated metathesis is the 14-electron intermediate (PCy_3)$RuCl_2$(=CR_2).[10] As demonstrated above, the surface silanols can interact with the free phosphine and the ruthenium complex, preventing thus the formation

of the $(PCy_3)_2RuCl_2(=CR_2)$ 16-electron species, the resting state of the catalyst. The rate of the second run for the reaction in the presence of SBA-15 is significantly lower than that of the first run and of the homogeneous reaction (conversion of 50% after 200 minutes; Figure 11b). The catalytic activity in the case of SBA-15/C_8 is completely inhibited in the second run, as no further conversion is observed. In contrast, in the case of the post-silylated sample, SBA-15*/C_8, the second run is proceeding at an appreciable rate, and has an activity similar to that in the presence of pristine SBA-15. Finally, in the case of SBA-15*, the catalyst remains very active with a conversion over 70% after 200 minutes. All these results suggest that once the first catalytic run is completed, fractions of the ruthenium or the phosphine must remain confined into the mesopores of the materials containing silanol groups, as observed in the ruthenium-containing samples, therefore leading to a decreased catalytic activity in solution with SBA-15 or a complete inhibition for SBA-15/C_8. However, in presence of TMS groups on the surface, the catalyst is relatively unaffected during the resting state and thus remains catalytically active.

Discussion

The recent results of Polarz and coworkers provided evidence that the Grubbs' catalyst was indeed deactivated by the presence of silica. Although several insights were obtained into the nature of the inorganic by-products, the exact nature of the surface remained uncertain. Our results demonstrate that although pristine SBA-15 reacts with Grubbs' first generation catalyst, the degradation is very slow, as shown by the ring-closing metathesis rate profile. It may be suggested that the slow diffusion of the organometallic ruthenium complex into the more hydrophilic pores of pristine SBA-15 limits the catalyst decomposition process. However, it is likely that the degradation of the catalyst is in part caused by the diffusion of the phosphine into the pores, and eventually of the

ruthenium-containing species. In our experiments, the Soxhlet extraction step that we performed allowed to focus our study on the chemisorbed species.‡ In every case, when the Grubb's catalyst is added to the mesoporous silica, the molar content in P observed is significantly higher than the molar content in Ru, indicative of relatively strong interactions occurring between the mesopore surface and the phosphine groups. In presence of oxygen during the extraction, phosphine species can easily be oxidized by ruthenium complexes, yielding phosphine oxide.[24] The adsorption of $O{=}PCy_3$ on pristine SBA-15 proved to be more efficient than the adsorption of PCy_3, as determined by EA (Table 3). Indeed, in the latter case, it was shown that only 15% of the available phosphorous atoms of a 4.8 mM solution of PCy_3 were chemisorbed on the surface, while in the case of the of $O{=}PCy_3$, more than 45% remained bound to the material surface. In order to gain more knowledge on this system, we also conducted a grafting of the second-generation Grubbs' catalyst under the same conditions as described before (see Experimental Section). With this other catalyst, the active species is known to be the NHC-containing 14-electron species without PCy_3, which is the most labile of the ligands. Since the active species in Grubbs II catalyst ($LRu(Cl)_2{=}CR_2$; L = N-heterocyclic carbene) does not contain any phosphorous and would thus be NMR silent if chemisorbed on the surface, the species observed by ^{31}P MAS NMR spectroscopy should arise mainly from the free phosphine. As can be observed in Figure 12, not only the ^{31}P MAS NMR spectrum of the hybrid SBA-15/Grubbs II material exhibits the same signals as the chemisorbed phosphine oxide and the tricyclohexylphosphonium, but the signal at 30.5 ppm is clearly more important for SBA-15/Grubbs II, which releases the phosphine more readily than SBA-15-Ru.[10] It can therefore be concluded that in the case of the Grubbs' first generation catalyst, most of the phosphine-containing species observed on silica do not remain bound to Ru.

Coating of SBA-15 silica with organosilane moieties, which was performed in order to cap the

silanol groups and make the pores more hydrophobic is believed to enhance markedly the diffusion of the Grubbs catalyst within the mesopores of the support. However, if the coverage is only partial, such as in the case of SBA-15/C_8, the degradation of the catalyst will be favored due to the presence of remaining surface silanols. Nevertheless, a more thorough coverage of the surface is possible, such as in the case of SBA-15* and SBA-15*/C_8 samples, to prevent the decomposition of the catalyst, although its diffusion in and out of the porous material is still possible, which will inevitably reduce its catalytic activity.

Conclusions

In this contribution, we concentrated on the solid-state characterization of differently functionalized-SBA-15 silica materials and the nature of their interactions with Grubbs I catalyst and the liberated phosphine ligands. From the above results, three hypotheses can thus be formulated regarding the SBA-15-Grubbs I catalyst interactions, which will complement the previous conclusions reported by Polarz[11]: 1) The pristine SBA-15 does indeed react with the Grubbs' catalyst and eventually will deactivate it. However, the catalyst is only slowly diffusing inside the hydrophilic mesopores of SBA-15 silica. Upon the formation of the active ruthenium catalyst, $(PCy_3)RuCl_2(=CR_2)$, free phosphine molecules may diffuse into the mesopores and bind to the surface either *via* the formation of a phosphonium or a phosphine adduct, which can further be oxidized in the presence of air; 2) In the presence of an octenyl chain, some part of the catalyst can transit into the mesopores and undergo ring-closing metathesis reaction, therefore reflecting the activity of the ruthenium species diffusing into the nanopores. However, this process is considered to act as a "trapping agent", terminating the homogeneous catalytic activity, once it has reacted with the residual silanols

accessible on the surface; and 3) Total passivation of the surface silanols using HMDS, with or without octenyl moieties on the surface, prevents the deactivation of the catalyst to occur, although it clearly slows down the olefin metathesis catalytic rate. To conclude, we believe that these findings contribute to a better understanding of the interactions between mesoporous silica supports and Grubbs' type catalysts, and that these new insights into the reactivity of phosphine-containing catalytic systems will be useful for further expanding the use of metal-phosphorous coordination chemistry on solid surfaces.

Experimental section

Materials. All grafting manipulations were carried out under an atmosphere of nitrogen, using standard Schlenk and glove box techniques. All support materials were outgassed under vacuum overnight, at 200 °C in the case of pure silica and at 50 °C for the hybrid organo-silicas. Dry toluene was distilled from sodium/benzophenone. Deuterated solvents were dried over NaK, degassed using freeze-pump thaw cycles, and purified by vacuum transfer.

SBA-15 silica support. Mesostructured SBA-15 silica material was prepared under aqueous acidic conditions using poly(alkylene oxyde)-based triblock copolymer Pluronic P123 ($EO_{20}PO_{70}EO_{20}$, MW = 5800, Aldrich) dissolved in a HCl solution (0.3 M).[12] The silica source was TEOS (ACROS 98%). The molar composition of the starting reaction mixture was 0.0012 P123 / 0.069 TEOS / 0.102 HCl / 6.771 H_2O. The reaction temperature with TEOS was fixed at 35 °C and the hydrothermal temperature was 100 °C. A typical preparation of the mesoporous 2-D silica is as follows: 6.71 g of P123 is dissolved in 121.87 g of distilled water and 3.72 g of 37 % wt HCl solution with stirring at 35 °C. After complete dissolution, 14.45 g of TEOS is added at once to the homogeneous clear solution. This mixture is left under vigorous stirring at 35 °C for 24 h. Subsequently, the mixture is aged at 100 °C for 24 h under

static conditions. The white precipitated product is filtered hot without washing and dried at 100 °C for 24 h in air. Surfactant-free mesoporous material is obtained after a brief ethanol/HCl washing and subsequent calcination at 550 °C in air.

Functionalization with octenyl-7-trichlorosilane (SBA-15/C_8). 7-octenyltrichlorosilane (Gelest 95%) (2 mL, 8.4 mmol) was added to a suspension of calcined SBA-15 (2.0 g) in dry toluene (60 mL) and then heated at 110 °C for 24 h. After cooling, the powder was filtered and washed with equivalent volumes of toluene and hexane. The resulting organic/inorganic hybrid material was dried at 85 °C overnight.

Passivation with hexamethyldisilazane (SBA-15 and SBA-15*/C_8).* Hexamethyldisilazane (Sigma-Aldrich 97%) (1.5 mL, 7.2 mL) was added to a suspension of silica (SBA-15 or SBA-15/C_8) (0.5 g) in toluene (30 mL). The reaction proceeded for 24 h at 110 °C. After cooling, the powder was filtered and washed with toluene and hexane.

Incorporation of the Grubbs I catalyst. To a suspension of a given silica support (0.5 g) in toluene (50 mL), Grubbs I catalyst (Sigma-Aldrich) (0.2 g, 0.24 mmol) was added and the mixture stirred for 2 h at room temperature. After filtration, the resulting material was washed in CH_2Cl_2 using Soxhlet extraction to obtain a grey/brown powder, except for SBA-15*/Ru which remained a white powder.

Incorporation of the phosphines. To a suspension of a given silica (0.15 g) in toluene (20 mL), tricyclohexylphosphine (Strem Chemical 97%) (0.086 mmol) was added and the resulting mixture was further stirred for 2h at room temperature. After filtration, the resulting powder was washed in CH_2Cl_2 using Soxhlet extraction and a white powder was obtained. The thus-obtained samples are designated as SBA-15/PCy_3 and SBA-15/C_8/PCy_3, respectively for SBA-15 and SBA-15/C_8 supports).

Incorporation of the phosphine oxide. To a suspension of SBA-15 silica (0.15 g) in toluene (20 mL), tricyclohexylphosphine oxide (Alfa Aesar, >99%) (0.086 mmol) was added and the resulting mixture was further stirred for 2h at room temperature. After filtration, the resulting powder was washed in

CH_2Cl_2 using Soxhlet extraction and a white powder was obtained. The thus-obtained sample is designated as SBA-15/$OPCy_3$.

Incorporation of the Grubbs II catalyst. To a suspension of SBA-15 silica (0.2 g) in toluene (30 mL), Grubbs II catalyst (Sigma-Aldrich) (0.09 g, 0.106 mmol) was added and the mixture stirred for 2 h at room temperature. After filtration, the resulting powder was washed in CH_2Cl_2 using Soxhlet extraction and a grey/brown powder was obtained. The sample is designated as SBA-15/Grubbs II.

Characterization. Solid state NMR spectra were recorded with a Bruker Avance 300 MHz spectrometer (^{13}C: 75.4 MHz; ^{31}P: 121.4 MHz; ^{29}Si: 59.6 MHz) equipped with a MAS probe head using 4mm ZrO_2 rotors and a sample spinning rate of 8000 Hz. The NMR spectra were recorded using cross-polarization/magic angle spinning (^{13}C) or magic angle spinning (^{29}Si and ^{31}P). Nitrogen adsorption-desorption isotherms were measured at liquid nitrogen temperature (-196 °C) using a Quantachrome Autosorb-1MP volumetric adsorption analyser. Before the measurements, the samples were outgassed under vacuum for 24h at 200 °C for purely siliceous SBA-15 and 80 °C for the functionalized organosilica materials. The Brunauer-Emmett-Teller (BET) equation was used to calculate the apparent surface area from adsorption data obtained at P/P_0 between 0.05 and 0.2. Total pore volume of micro-mesopores was calculated from the amount of nitrogen adsorbed at P/P_0 = 0.95, assuming that adsorption on the external surface was negligible compared to adsorption in pores. Cumulative pore volumes and pore size distributions were determined by using *non-local density functional* (NLDFT) methods considering sorption of nitrogen at -196 °C in cylindrical silica pores.[14-18,25] Both the kernel of equilibrium NLDFT isotherms (desorption branch) and the kernel of (metastable) NLDFT adsorption isotherms (adsorption branch) were applied for pore width determination.[25,26] For comparison, the pore size distributions were also calculated by analyzing the adsorption branch of the isotherm using the Barret-Joyner-Halenda (BJH) method.

Thermogravimetry-differential thermal analysis (TG-DTA) measurements were performed using a Netzsch STA 449C thermogravimetric analyzer. The analyses were carried out under air flow at a heating rate of 10 °C/min. Infrared spectra spectra were recorded using a Thermo-Nicolet Magna 850 FTIR spectrometer with a narrow band MCT detector and a diamond ATR Golden-Gate accessory (Specac Ltd., London). The spectra were obtained from 128 scans with a $4cm^{-1}$ resolution. The elemental analyzes were performed at the Guelph Chemical Laboratories Ltd, Guelph, Ontario, Canada. Carbon, Hydrogen and Nitrogen analysis was performed by the combustion method using a Carlo Erba Model 1108 CHNS Analyzer. In this method, a known amount of sample (~2 to 3 mg) was combusted at 1000° C in the presence of an oxidant catalyst in an oxidation quartz reactor tube. The resulting product gases were passed through the catalytic reduction chamber. The final product gases (CO_2, H_2O and N_2) were analyzed by gas chromatography using a thermal conductivity detector. Certified NIST traceable standards (acetanilide, cyclohexanone) with known % C, % H, % N were also analyzed under the same experimental conditions from which the % of CHN were calculated in the sample. The method error limit on Carbon is +/- 0.5% of absolute value, Hydrogen is +/- 0.4% absolute value and Nitrogen is +/- 0.3% absolute value. Ruthenium and Phosphorus analyses were performed by a Varian Liberty Series II ICP-OES. A small amount of sample (5-10 mg) was digested in concentrated nitric acid for 2 hours. The digestant solution was transferred into a volumetric flask and diluted to known volume with de-ionized water. Calibration standards of Ru (1, 5, 10 mg/L with correlation coefficient > 0.999), and P (2, 4, 10, 25, 50 mg/L (with correlation coefficient > 0.999) were used for the analysis of Ru and P in the sample by analysis with Inductively Coupled Plasma instrument.

Catalytic tests. To a suspension of 10 mg of silica in 2.5 mL dry toluene, modified or not, the Grubbs I catalyst (1.7 mg, 0.002 mmol, 0.81mM) was added and the mixture stirred at room temperature. After 10 minutes, diethyldiallylmalonate (Alfa Aesar, 98%) (40 μL, 0.17 mmol) was added and stirring

proceeded for 5 hours. After this first run, for the recycling, the same volume (40 μL) of diethyldiallylmalonate was added and then stirred for an additional 5 hours. The solution became orange when the malonate was added. Only two organic species were observed during the reaction using NMR spectroscopy and gas chromatography/mass spectrometry (GC-MS), which corresponded to the diethyldiallylmalonate and its cyclisation product. The product/reagent ratios were recorded on a ThermoFisher Scientific Trace GC Ultra coupled with MS ion trap ITQ 900 in Chemical Ionisation**.** The conversion of diethyldiallylmalonate was measured as a function time by quantifying the opened/cyclized olefin ratio.

[‡]*Footnotes*. Some leaching of Ru species may occur during the Soxhlet extraction step, as previously discussed by Polarz et al. [11] and also observed by us. However, in the present study, leaching of Ru was not quantified as we deliberately concentrated on the characterization of the strongly adsorbed species.

Acknowledgements

The authors acknowledge financial support from the National Science and Engineering Research council (Canada), the Canadian Foundation for Innovation and the Fonds québécois de la recherche sur la nature et les technologies (Province of Quebec). The authors wish to thank Prof. Michel Pézolet and Jean-François Rioux for the access to ATR-IR measurements (Department of Chemistry, Université Laval).

[1] W. L. Truett, D. R. Johnson, I. M. Robinson, B. A. Montague *J. Am. Chem. Soc*. **1960**, *82*, 2337-2340.

[2] J. S. Murdzek, R. R. Schrock, *Organometallics* **1987**, *6*, 1373-1374.

[3] P. Schwab, M. B. France, J.W. Ziller, R. H. Grubbs, *Angew. Chem. Int. Ed.* **1995**, *34*, 2039-2041.

[4] Some recent review articles : a) A. M. Lozani-Vila, S. Monsaert, A. Bajek, F. Verpoort, *Chem. Rev.* **2010**, *110*, 4865-4909; b) T. J. Donohoe, T. J. C. O'Riordan, C. P. Rosa, *Angew. Chem. Int. Ed.* **2009**, *48*, 1014-1017; c) G. C. Vougioulakakis, R. H. Grubbs, *Chem. Rev.* **2010**, *110*, 1749-1787; d) C. Samojlowicz, M. Bieniek, K. Grela, *Chem. Rev.* **2009**, *109*, 3743-3482.

[5] a) A. Mendonca, in *Power of Functional Resins in Organic Synthesis*; J. Tulila-Puche and F. Albericio, Eds.; VCH-Wiley, Weinheim, Germany, 2008, pp 227-243; b) R. Anwander, "Immobilization of Molecular Catalysts", In *Handbook of Heterogeneous Catalysis*, *2nd edition*, G. Ertl, H. Knötzinger, F. Schüth and J. Weitkamp, Eds., VCH-Wiley, Weinheim, 2008, Vol. 1, pp 583-614; c) C. A. McNamara, M. J. Dixon, M. Bradley, *Chem. Rev.* **2002**, *102*, 3275-3300; d) M. R. Buchmeister, *Chem. Rev.* **2009**, *109*, 303-321; e) K. McEleney, D. P. Allen, A. E. Holliday, C. M. Crudden, *Org. Lett.* **2006**, *8*, 2663; f) C. M. Crudden, K. McEleney, S. L. MacQuarrie, A. Blanc, M. Sateesh, J. D. Webb, *Pure Appl. Chem.* **2007**, *79*, 247-260; g) X. Feng, G. E. Fryxell, L. Q. Wang, A. Y. Kim, J. Liu, K. M. Kemner. *Science* **1997**, *276*, 923-926.

[6] a) J. Y. Ying, C. P. Mehnert, M. S. Wong, *Angew. Chem. Int. Ed.* **1999**, *38*, 56-77; b) C. E. Song, S. Lee, *Chem. Rev.* **2002**, *102*, 3495-3524; c) D. E. De Vos, M. Dams, B. F. Sels, P. A. Jacobs, *Chem. Rev.* **2002**, *102*, 3615-3640; d) A. P. Wight, M. E. Davis, *Chem. Rev.* **2002**, *102*, 3589-3614; e) A. Taguchi, F. Schuth, *Microporous Mesoporous Mater.* **2005**, *77*, 1-45; f) A. Corma, H. Garcia, *Adv. Synth. Catal.* **2006**, *348*, 1391-1412; g) S. Minakata, M. Komatsu, *Chem. Rev.* **2009**, *109*, 711-724.

[7] S. T. Nguyen, R. H. Grubbs, *J. Organomet. Chem.* **1995**, *497*, 195-200.

[8] K. Melis, D. De Vos, P. Jacobs, F. Verpoort, *J. Mol. Catal. A : Chem.* **2001**, *169*, 47-56.

[9] a) M. Mayr, M. R. Buchmeiser, K. Wurst, *Adv. Synth. Catal.* **2002**, *344*, 712-719; b) J. O. Krause, S. Lubbad, O. Nuyken, M. R. Buchmeiser, *Adv. Synth. Catal.* **2003**, *345*, 996-1004; c) X. Elias, R. Pleixats, M. W. C. Man, J. J. E. Moreau, *Adv. Synth. Catal.* **2006**, *348*, 751-762; d) F. Michalek, W. Bannwarth, *Helv. Chim. Acta* **2006**, *89*, 1030-1037; e) K. Vehlow, S. Maechling, K. Köhler, S. Blechert, *J. Organomet. Chem.* **2006**, *691*, 5267-5277; f) J. Lim, S. S. Lee, S. N. Riduan, J. Y. Ying, *Adv. Synth. Catal.* **2007**, *349*, 1066-1076; g) X. Elias, R. Pleixats, M. W. C. Man, J. J. E. Moreau, *Adv. Synth. Catal.* **2007**, *349*, 1701-1713; h) X. Elias, R. Pleixats, M. W. C. Man, *Tetrahedron* **2008**, *64*, 6770-6781; i) J. Lim, S. S. Lee, J. Y. Ying, *Chem. Commun.* **2010**, *46*, 806-808; j) D. Bek, N. Zilkova, J. Dedecek, J. Sedlacek, H. Balcar, *Top. Catal.* **2010**, *53*, 200-209; k) D. P. Allen, M. M. Van Wingerden, R. H. Grubbs, *Org. Lett.* **2009**, *11*, 1261-1264; l) B. Van Berlo, K. Houthoffd, B. F. Sels, P. A. Jacobs, *Adv. Synth. Catal.* **2008**, *350*, 1949-1953; m) D. Fischer, S. Blechert, *Adv. Synth. Catal.* **2005**, *347*, 1329-1332; (n) L. Li, J.-L. Shi, *Adv. Synth. Catal.* **2005**, *347*, 1745-1749; n) F. Michalek, D. Mädge, J. Rühe, W. Bannwarth, *J. Organomet. Chem.* **2006**, *691*, 5172-5180; o). J. Lim, S. S. Lee, S. N. Riduan, J. Y. Ying, *Adv. Synth. Catal.* **2007**, *349*, 1066-1076.

[10] M. S. Sanford, M. Ulman, R. H. Grubbs, *J. Am. Chem. Soc.* **2001**, *83*, 3306-3311.

[11] S. Polarz, B. Völker, F. Jeremias, *Dalton Trans.* **2010**, *39*, 577-584.

[12] M. Choi, W. Heo, F. Kleitz, R. Ryoo, *Chem. Commun.* **2003**, 1340-1341.

[13] a) S. A. Kozlova, S. D. Kirik, *Microporous Mesoporous Mater.* **2010**, *133*, 124-133; b) X. S. Zhao, G. Q. Lu, A. K. Whittaker, G. J. Millar, H. Y. Zhu, *J. Phys. Chem. B* **1997**, *101*, 6525-6531.

[14] A. V. Neimark, K. S. W. Sing, M. Thommes, in *Handbook of Heterogeneous Catalysis, 2nd edition*, G. Ertl, H. Knözinger, F. Schüth, J. Weitkamp, Eds., VCH-Wiley, Weinheim, 2008, pp 721-738.

[15] a) M. Thommes, in *Nanoporous Materials; Science and Engineering*; G. Q. Lu,X. S. Zhao, Eds., Imperial College Press, London, U.K., 2004, pp 317-364. b) M. Thommes, *Chemie Ingenieur Technik* **2010**, *82*, 1059-1073.

[16] a) C. P. Jaroniec, M. Kruk, M. Jaroniec, A. Sayari, *J. Phys. Chem. B* **1998**, *102*, 5503-5510. b) V. Antochshuk, M. Jaroniec, *J. Phys. Chem. B* **1999**, *103*, 6252-6261. c) R. Anwander, I.Nagl, M. Widenmeyer, G. Engelhardt, O. Groeger, C. Palm, T. Röser, *J. Phys. Chem. B*, **2000**, *104*, 3532–3544

[17] a) Q. Wang, E. Jordan, D. F. Shantz, *J. Phys. Chem.* C **2009**, *113*, 18142–1815. b) S. L. Hruby, B. H. Shanks, *J. Catal.* **2009,** 263, 181–188.

[18] F. Kleitz, F. Bérubé, R. Guillet-Nicolas, C.-M. Yang, M. Thommes, *J. Phys. Chem. C* **2010**, *114*, 9344-9355.

[19] a) M. Choi, F. Kleitz, D. Liu, H. Y. Lee, W.-S. Ahn, R. Ryoo, *J. Am. Chem. Soc.* **2005**, 127, 1924-1932. b) R. Palkovits, C.-M. Yang, S. Olejnik, F. Schüth, *J. Catal.* **2006**, *243*, 93-98. c) A. Rumplecker, F. Kleitz, E. L. Salabas, F. Schüth, *Chem. Mater.* **2007**, *19*, 485-496.d) M. Wainer, L. Marcoux, F. Kleitz, *J. Mater. Sci.***2009,** *44*, 6538–6545. e) R. Guillet-Nicolas, L. Marcoux, F. Kleitz, *New. J. Chem.* **2010**, 34, 355–366.

[20] R. Palkovits, D. Artl, H. Stepwoska, F. Schüth, *Chem. Eur. J.* **2009**, *15*, 9183-9190.

[21] S. A. Alekseev, V. N.,Zaitsev, J. Fraissard, *Chem. Mater.* **2006**, *18*, 1981-1987.

[22] I. Batonneau-Gener, A. Yonli, A. Trouvé, S. Mignard, M. Guidotti, Sgobba, M. In *Separation Science and technology*; Taylor and Francis group, LLC, 2010, Vol. 45, pp 768-775.

[23] B. Hu, I. D. Gay, *Langmuir* **1995**, *11*, 3845-3847.

[24] M. M. Taqui Khan, D. Chartterjee, M. R. H. Siddiqui, S. D. Bhatt, H. C. Bajaj, K. Venkatasubramanian, M. A. Moiz, *Polyhedron* **1993**, *12*, 1443-1451.

[25] P. I. Ravikovitch, A. V. Neimark, *J. Phys. Chem. B* **2001**, *105*, 6817.

[26] A. V. Neimark, P. I. Ravikovitch, *Microporous Mesoporous Mater.* **2001**, *44*, 697.

Tables

Table 1: Physico-chemical properties derived from N_2 sorption measurements for the parent pure silica SBA-15 material and the differently functionalized samples.

Materials	S_{BET} [a] $[m^2.g^{-1}]$	V_t [b] $[cm^3.g^{-1}]$	$NLDFT_{ads}$ [c] [nm]	$NLDFT_{des}$ [d] [nm]	$BJH_{ads.}$ [nm]
SBA-15	875	1.26	8.15	8.5	8.6
SBA-15/C_8	534	0.81	7.3	7.6	7.4
SBA-15*	693	1.03	7.6	7.9	8.0
SBA-15*/C_8	370	0.59	7.05	7.05	7.15

[a] S_{BET}, apparent BET specific surface area deduced from the isotherm analysis in the relative pressure range from 0.05 to 0.20. [b] V_t, total pore volume taken at relative pressure $P/P_0 = 0.95$. [c] $NLDFT_{ads}$, the primary mesopore diameter estimated using NLDFT method. The model used for NLDFT evaluation was N_2 adsorbed on silica with cylindrical pores considering the adsorption branch (model of metastable adsorption). [d] $NLDFT_{des}$, the primary mesopore diameter estimated using NLDFT method. The model used for NLDFT evaluation was N_2 adsorbed on silica with cylindrical pores considering the desorption branch (equilibrium sorption model).

Table 2. Weight loss for the different samples measured up to 700 ^{o}C by thermogravimetric analyses.

Materials	*Mass Loss [%]*
SBA-15-Ru	4.0
SBA-15*	3.0
SBA-15*-Ru	4.5
SBA-15/C_8	15.0
SBA-15/C_8-Ru	19.0
SBA-15*/C_8	14.0
SBA-15*/C_8-Ru	12.0
SBA-15-PCy_3	5.5
SBA-15/C_8-PCy_3	16.5
SBA-15-$OPCy_3$	9.0

Table 3. Elemental analysis data for the various samples studied (N.D. stands for not detected).

Materials	*%C*	*%H*	*%P*	*%Ru*
SBA-15-Ru	2.88	0.55	0.32	0.34
SBA-15/C_8	10.50	2.80	-	-
SBA-15/C_8-Ru	12.87	3.54	0.23	0.27
SBA-15*/C_8	14.13	3.38	-	-
SBA-15*/C_8-Ru	12.31	2.33	0.083	0.025
SBA-15*	6.20	0.97	-	-
SBA-15*-Ru	6.22	0.99	0.025	N.D.
SBA-15-PCy_3	4.30	1.29	0.26	-
SBA-15/C_8-PCy_3	10.90	2.07	0.81	-
SBA-15-$OPCy_3$	6.62	1.67	0.97	-

Schemes

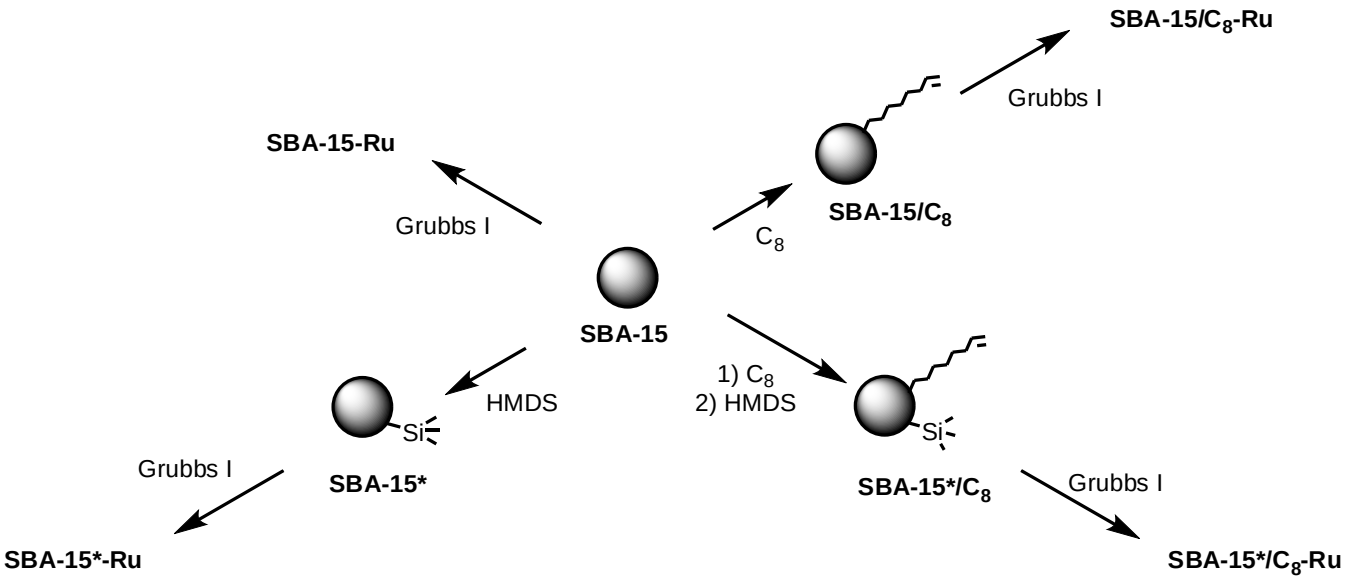

Scheme 1. Synthesis pathways for the different functionalized mesoporous materials (C_8 = CH_2=CH(CH_2)$_6$$SiCl_3$).

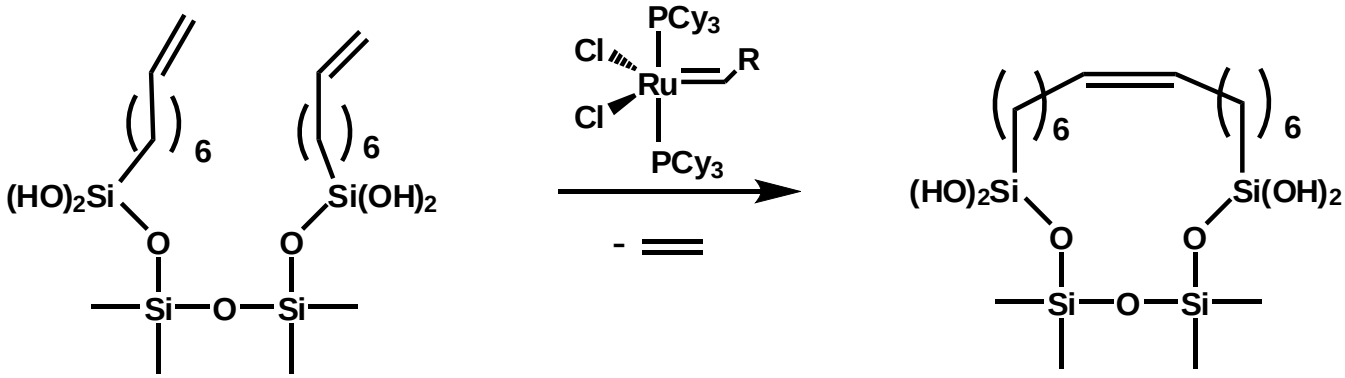

Scheme 2. Ring-closing metathesis of the octenyl chains on SBA-15/C_8 and SBA-15*/C_8.

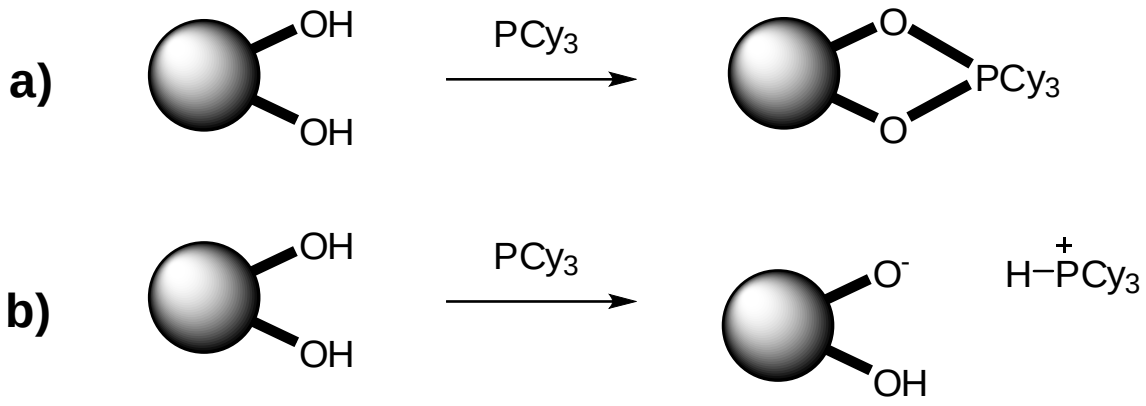

Scheme 3. Possible interaction modes between PCy_3 and the silanols present on the pore surface of the silica materials.

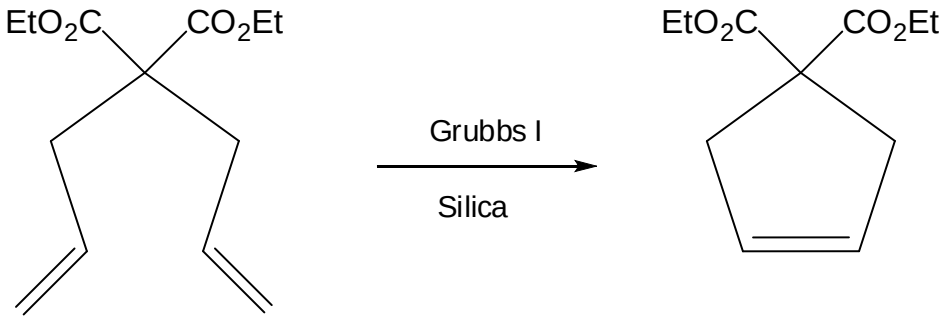

Scheme 4**.** Ring-closing metathesis of diethyldiallylmalonate into 3-cyclopentene-1,1-dicarboxylic acid-1,1-diethylester.

Figures

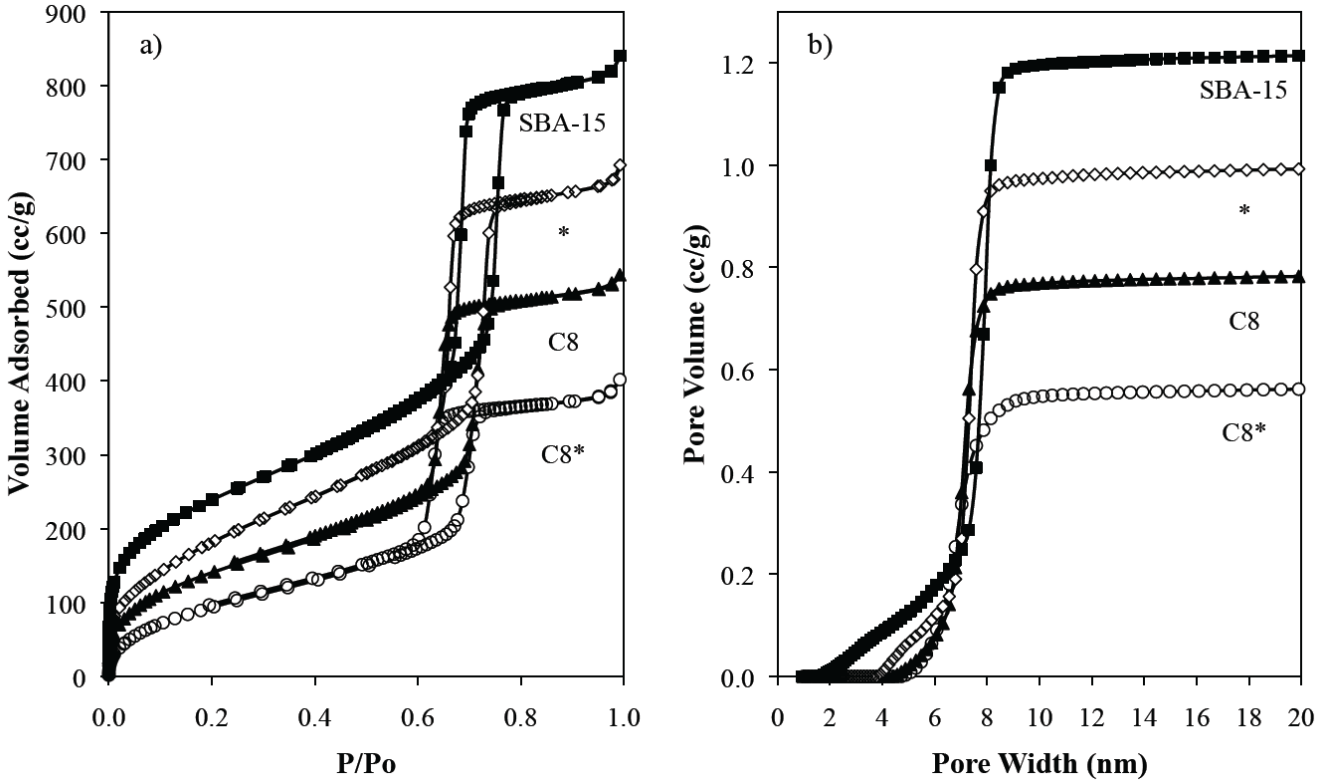

Figure 1. a) N_2 adsorption-desorption physisorption isotherms measured at -196 °C for the parent SBA-15 silica and the different organo-functionalized materials; b) respective NLDFT cumulative pore volume plots (NLDFT kernel of metastable adsorption isotherms – adsorption branch)

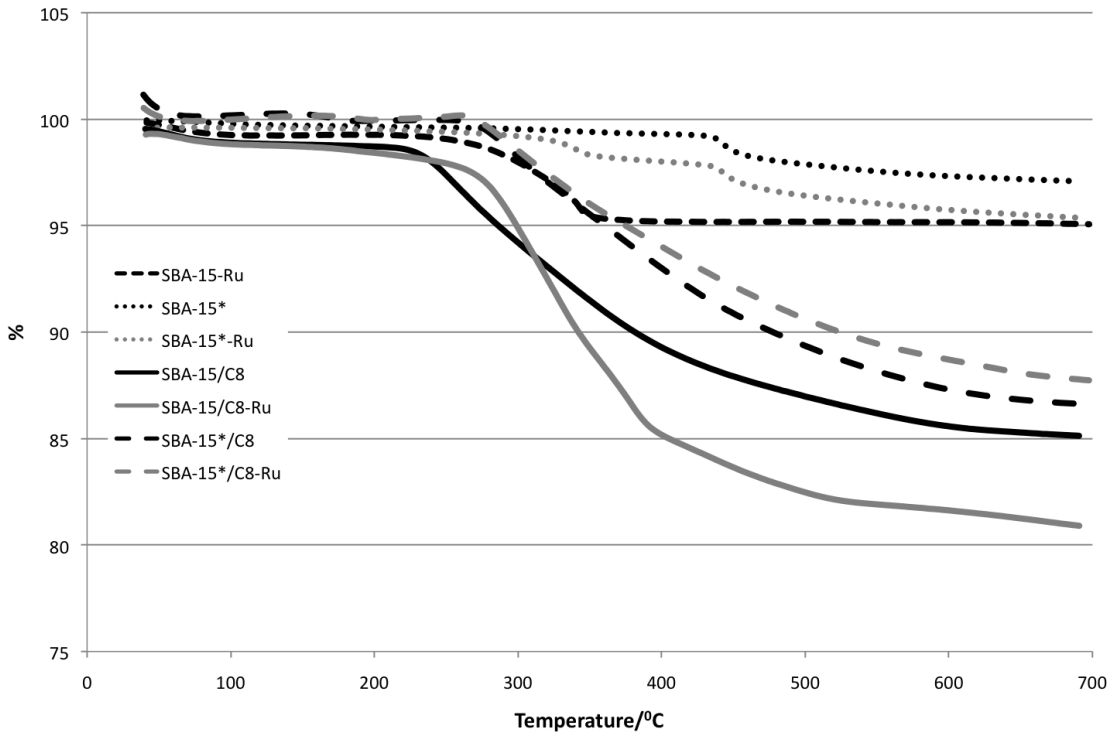

Figure 2. Thermogravimetric analysis weight loss profiles for the studied mesoporous materials (as indicated).

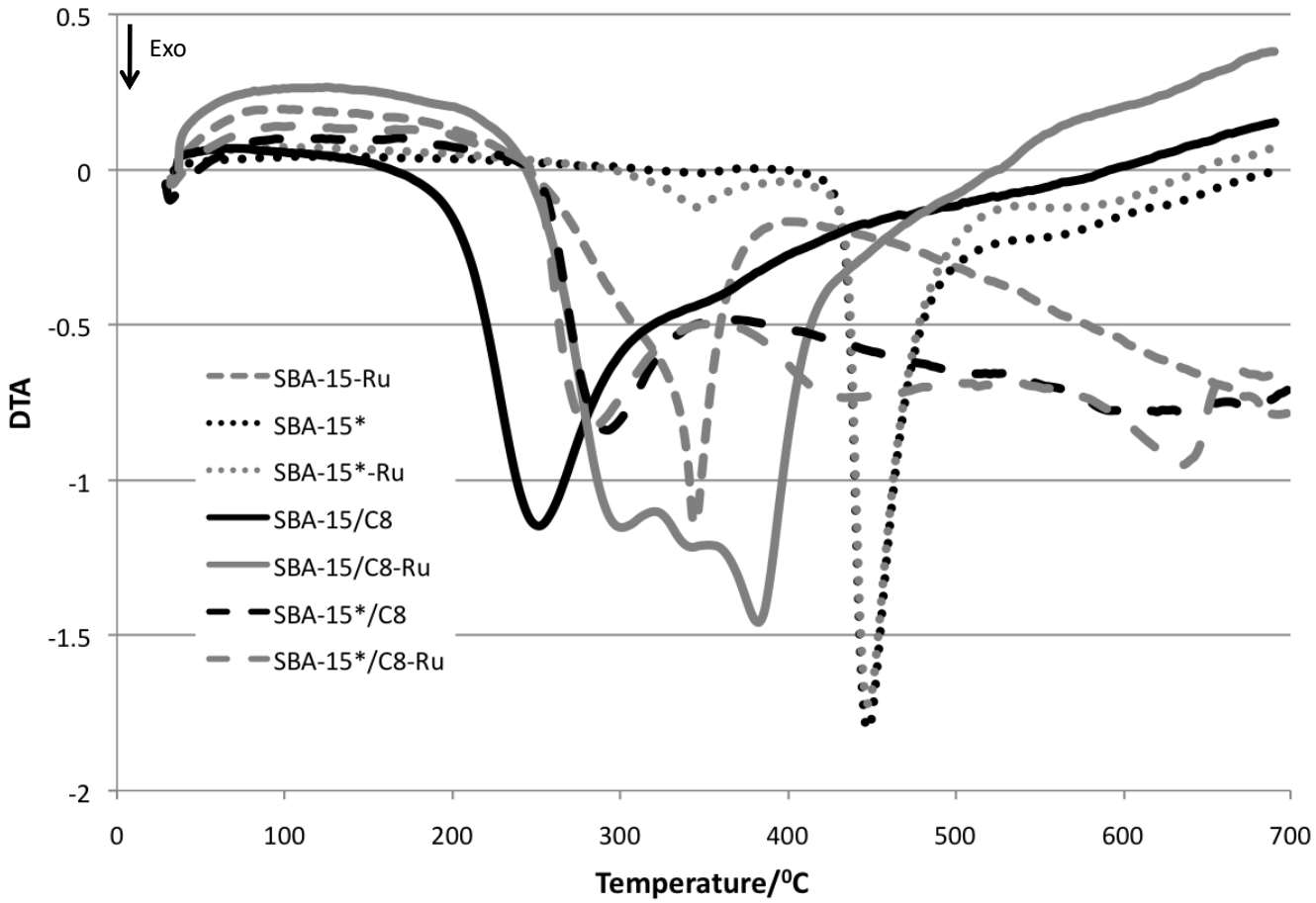

Figure 3. Differential thermal analysis profiles of the studied materials (as indicated).

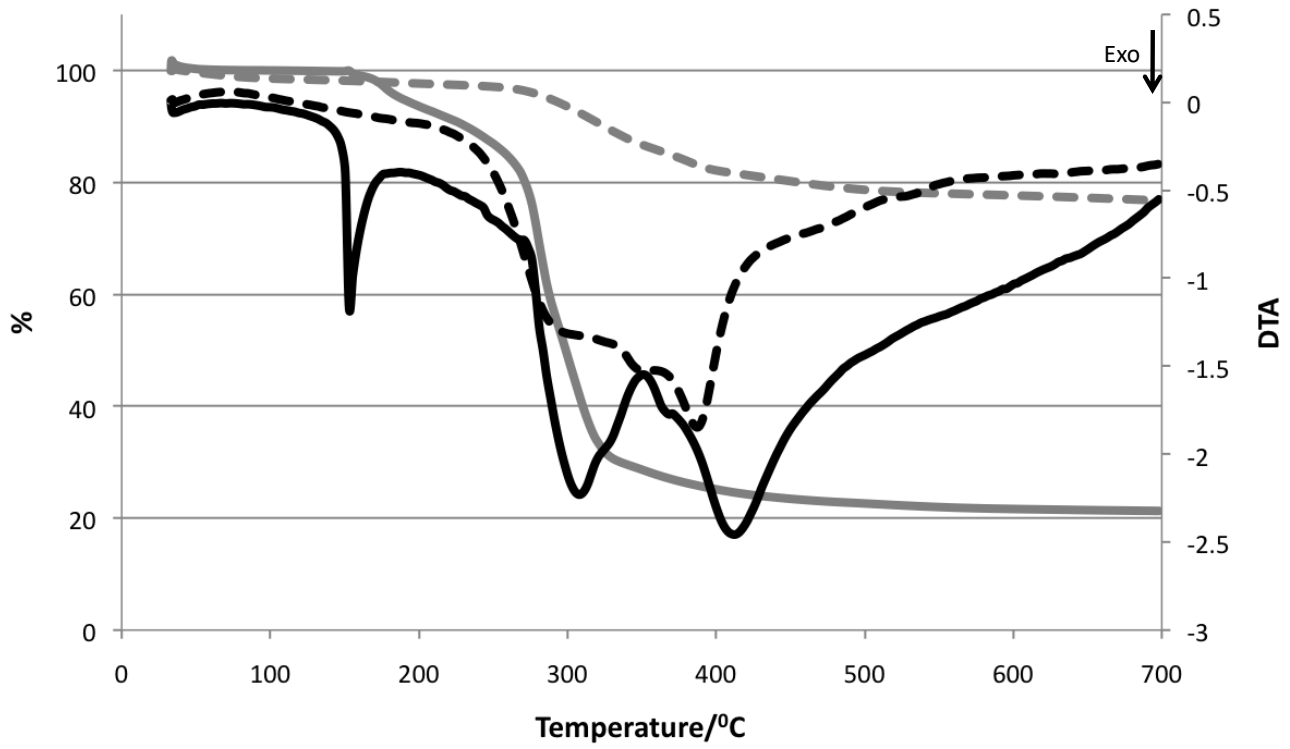

Figure 4. Thermogravimetric analysis weight loss profile (black) and coupled differential thermal analysis plot (gray) for the Grubbs I catalyst (straight line) and SBA-15/C_8-Ru (dashed line).

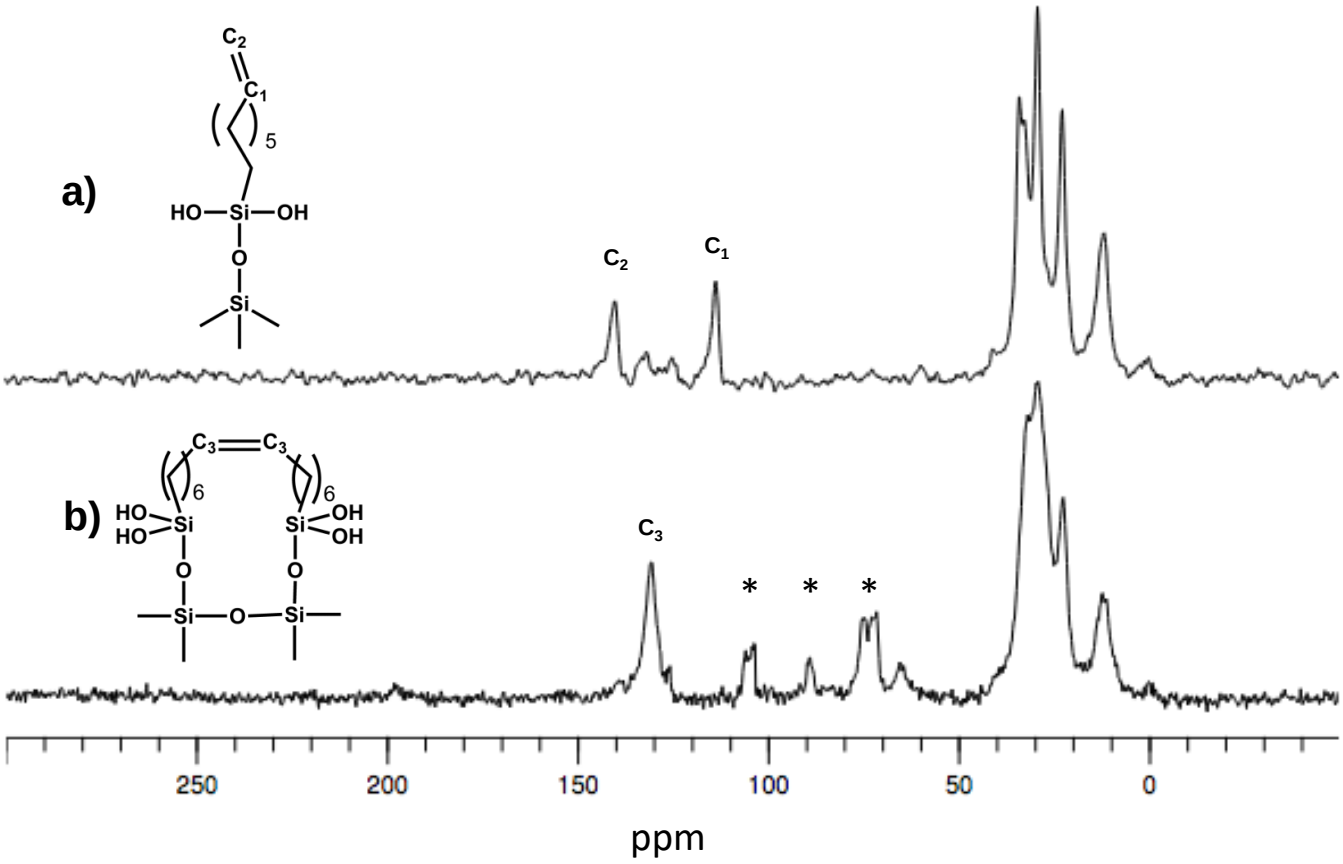

Figure 5. ^{13}C CP/MAS NMR spectra of a) SBA-15/C_8 and b) SBA-15/C_8-Ru. *denotes an unidentified resonance. Grafting of the octenylsilane moieties is represented as a monopodal attachment to the surface, for simplification. Both bi- and tripodal anchoring modes are also likely to occur.

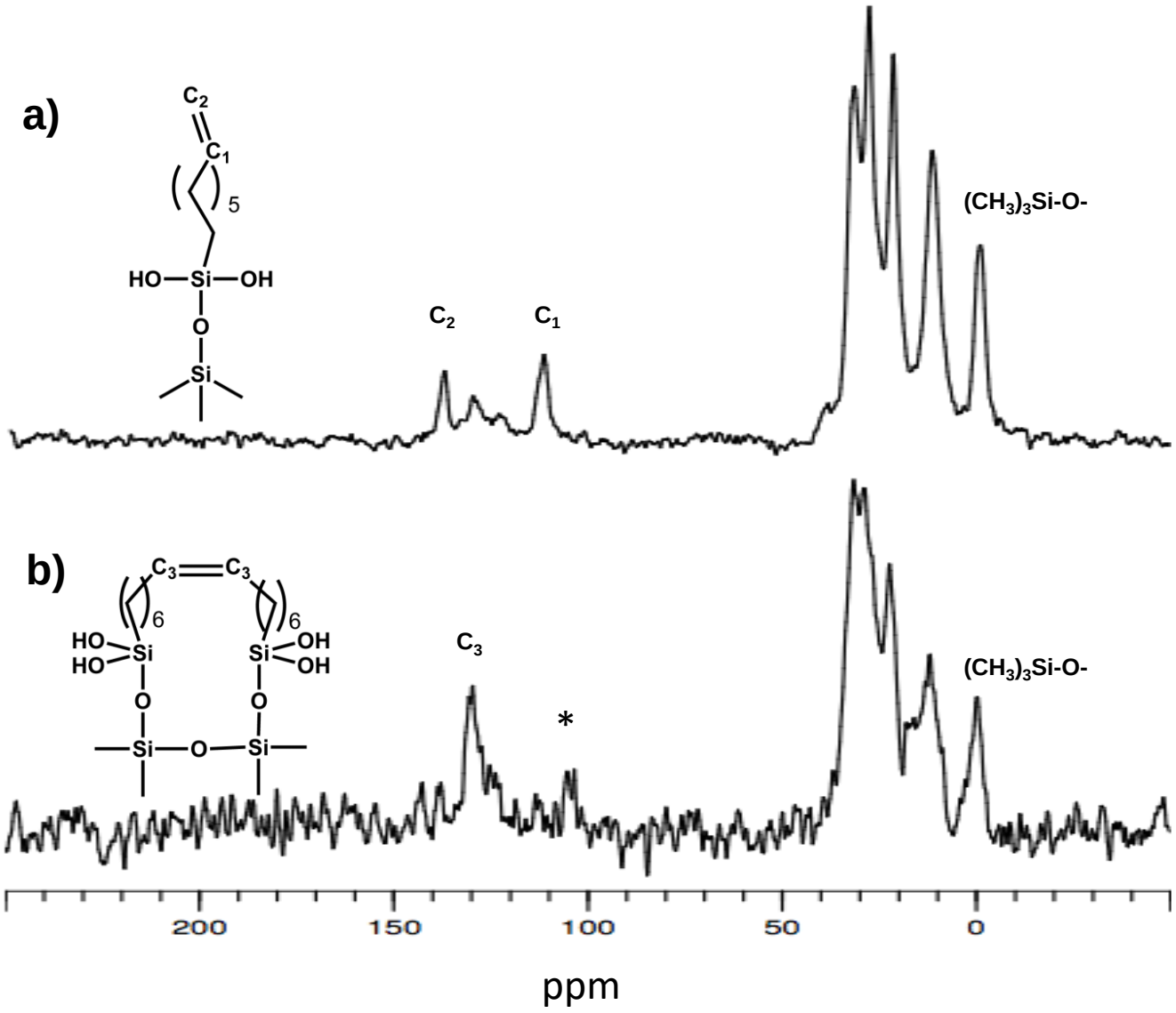

Figure 6. ^{13}C CP/MAS NMR spectra of a) SBA-15*/C_8 and b) SBA-15*/C_8-Ru. *denotes an unidentified resonance. Grafting of the octenylsilane moieties is represented as a monopodal attachment mode to the surface, for simplification. Both bi- and tripodal anchoring modes are also likely to occur.

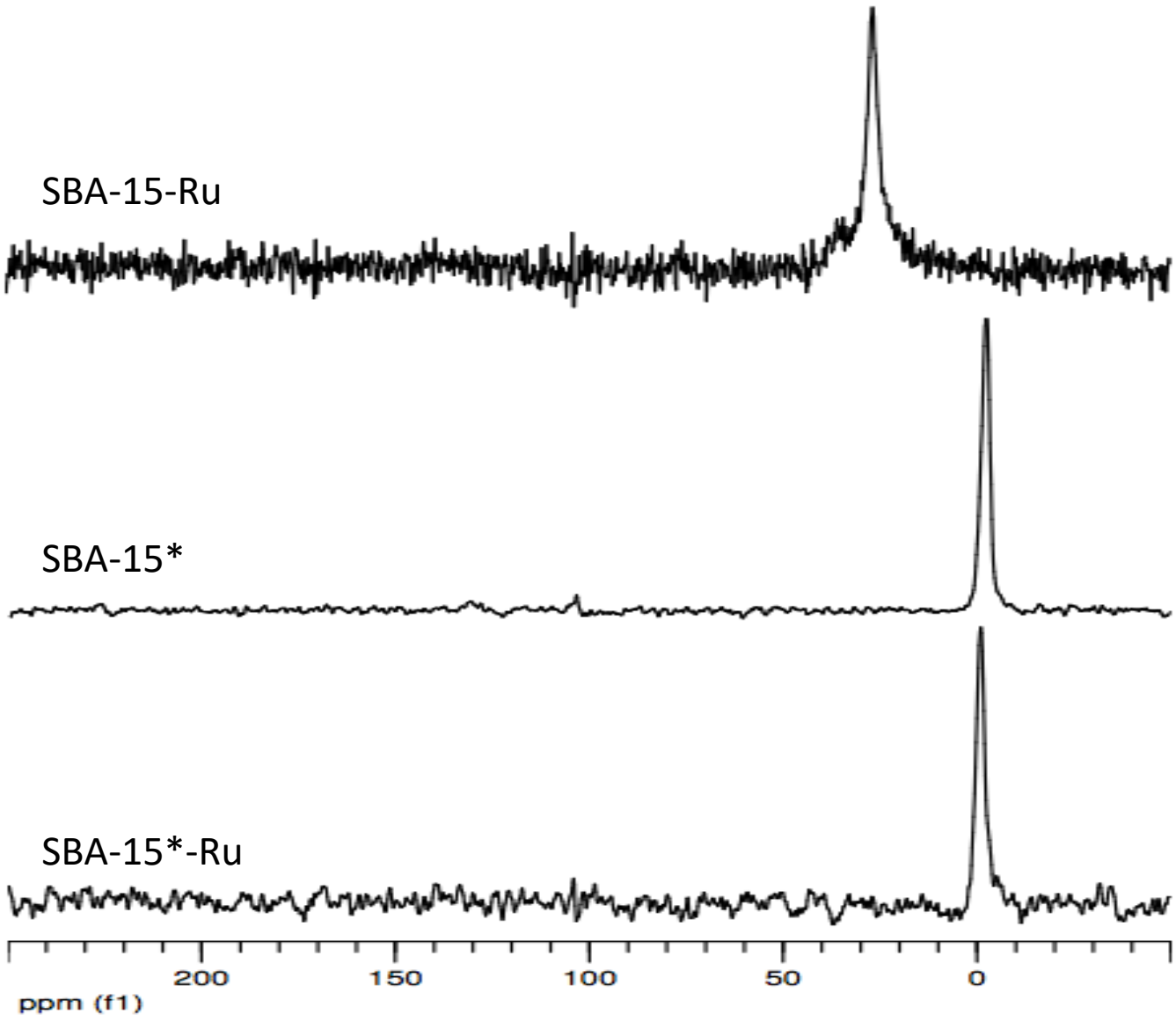

Figure 7. ^{13}C CP/MAS NMR spectra of a) SBA-15-Ru, b) SBA-15*, and c) SBA-15*-Ru.

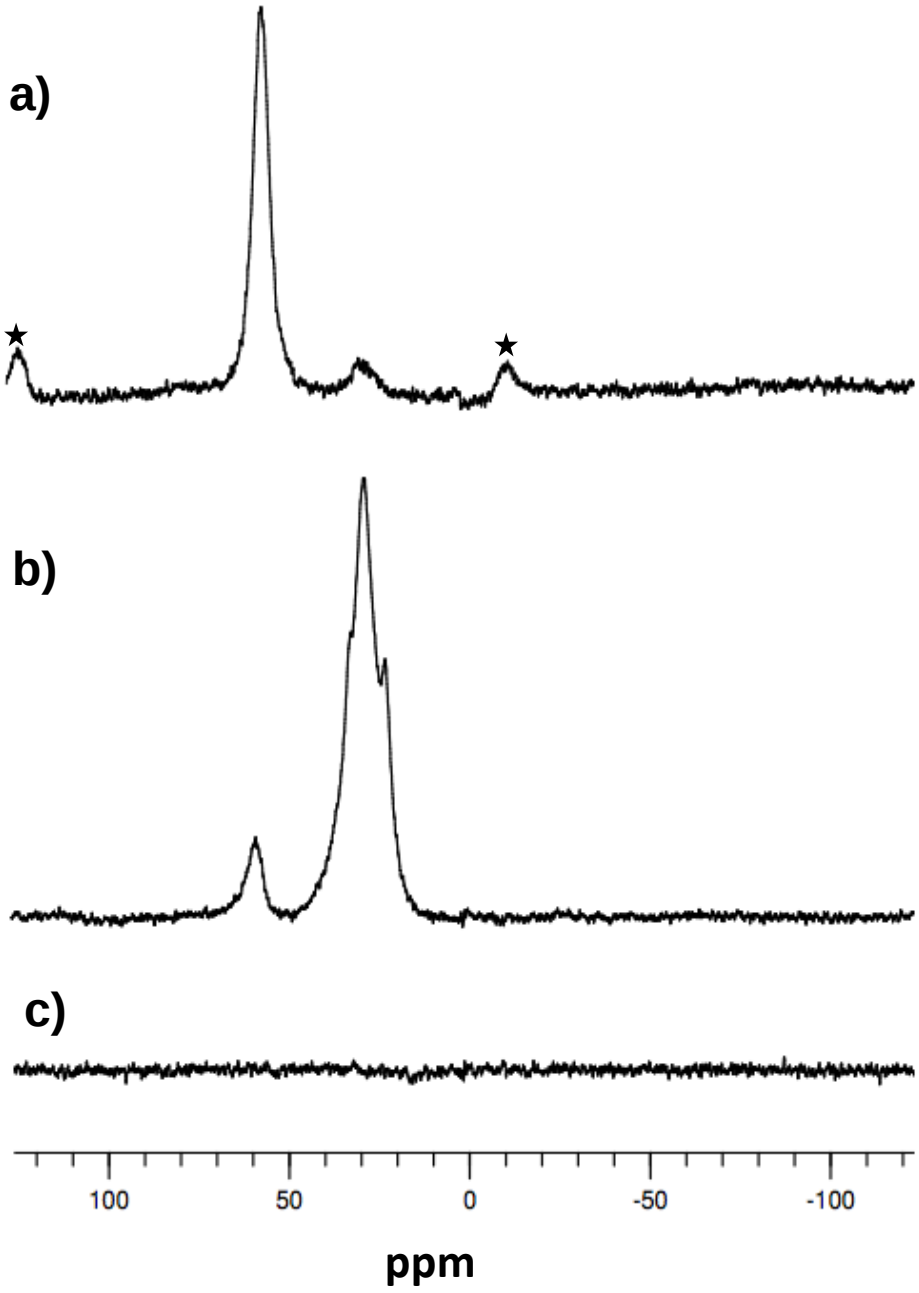

Figure 8. ^{31}P MAS NMR spectra of a) SBA-15-Ru, b) SBA-15/C_8-Ru, and c) SBA-15*/C_8-Ru. *denotes spinning side-bands.

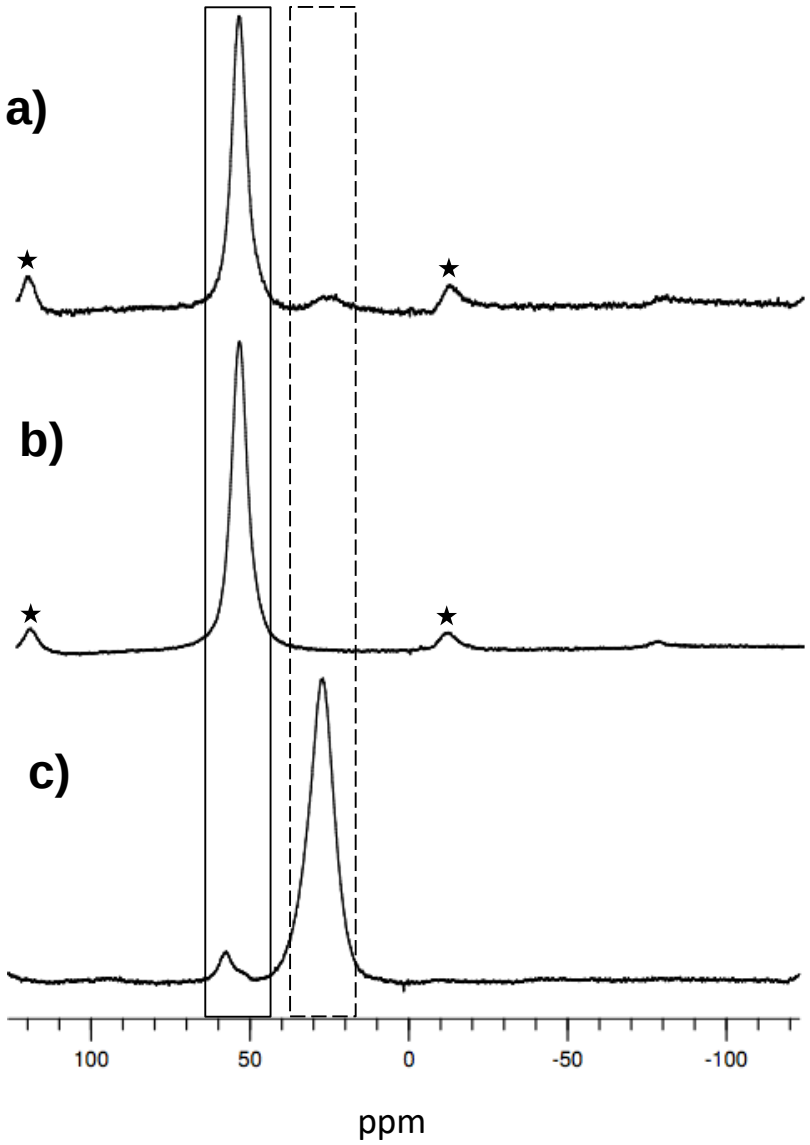

Figure 9. ^{31}P MAS NMR spectra of SBA-15 with a) PCy_3, b) $OPCy_3$, and c) of SBA-15/C_8 with PCy_3. *denotes spinning side-bands.

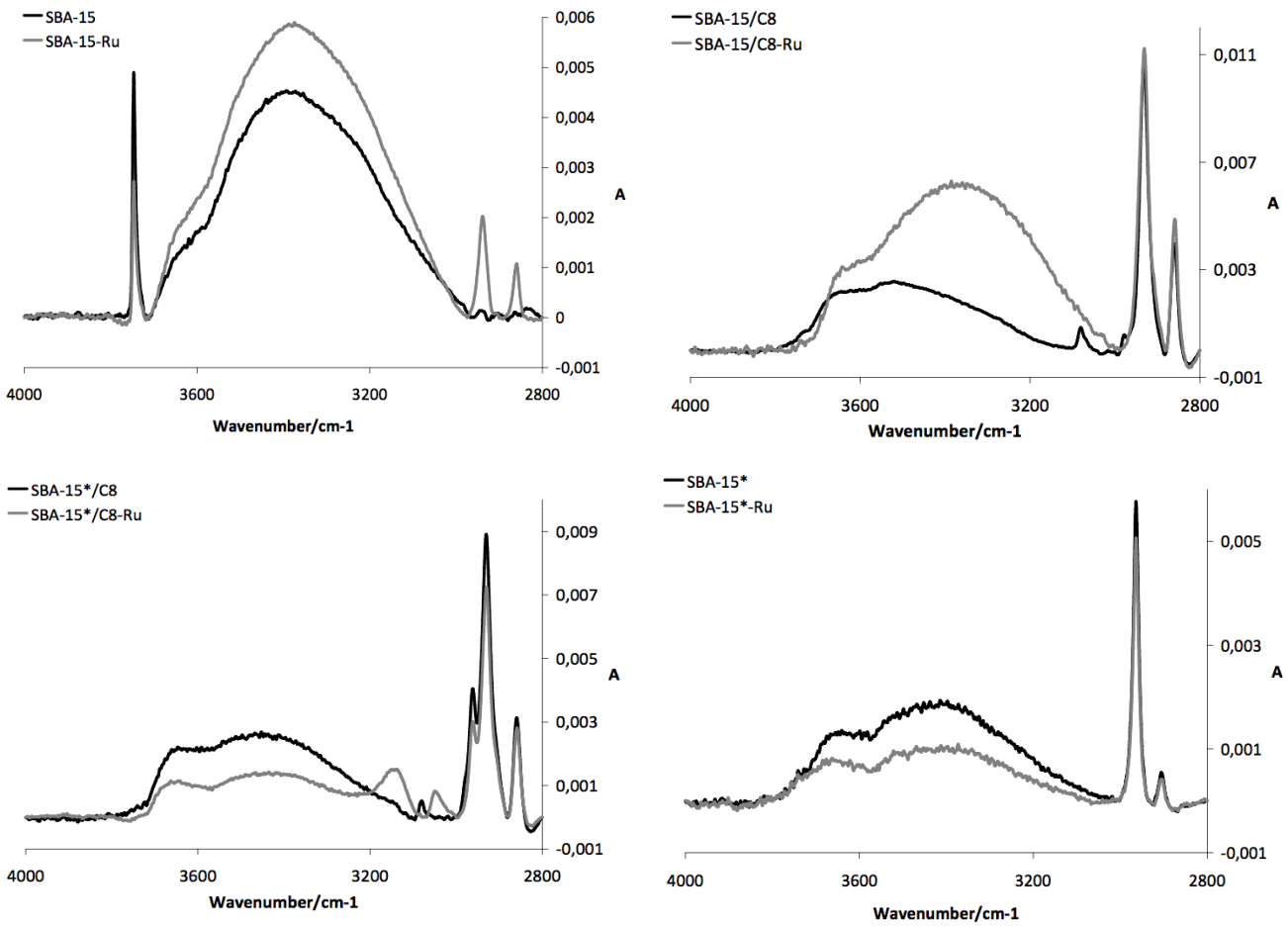

Figure 10. Infra-red spectra showing the region corresponding to the O-H and C-H frequencies of the studied materials, as indicated, obtained using attenuated total reflection infrared spectroscopy (ATR-IR).

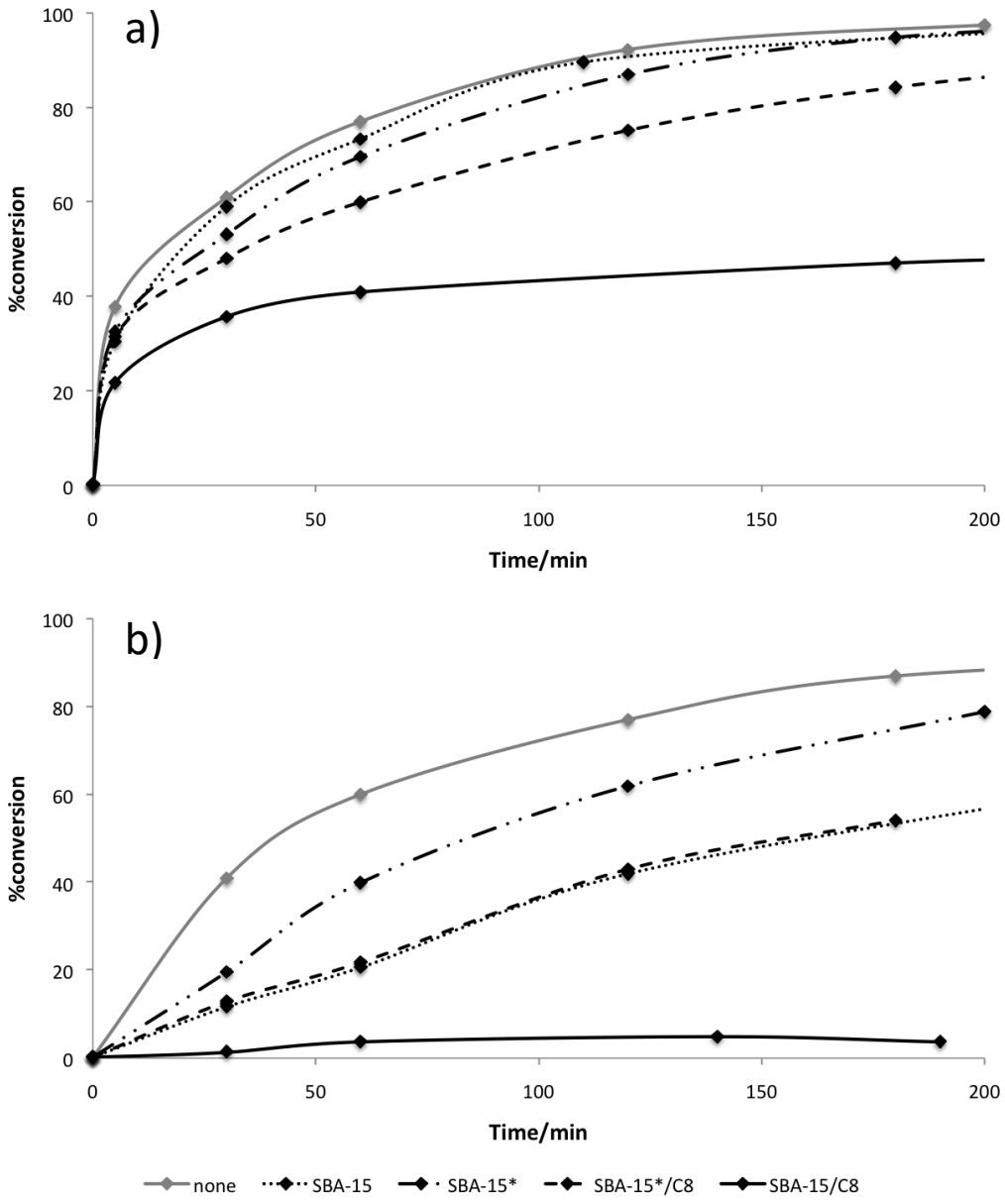

Figure 11. a) Conversion of 80 equivalents of diethyldiallylmalonate into 3-cyclopentene-1,1-dicarboxylic acid-1,1-diethylester by ring-closing metathesis in the presence of one equivalent of Grubbs' first generation and organo-functionalized or pristine SBA-15. b) Rate profile after the addition of a second 80 equivalents of diethyldiallylmalonate 300 minutes after the first addition.

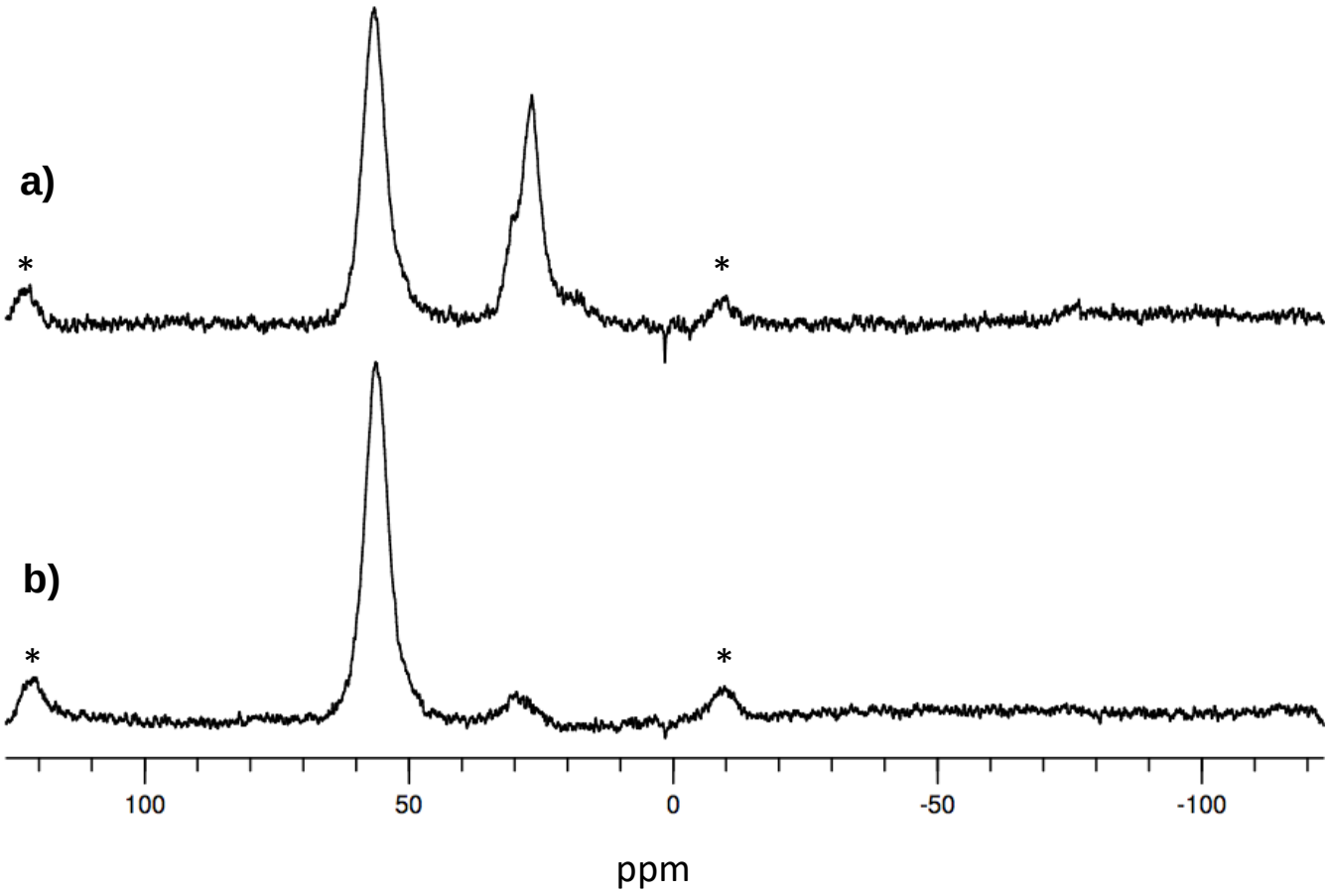

Figure 12. ^{31}P MAS NMR spectra of a) SBA-15 silica in the presence of Grubbs' second generation catalyst and b) SBA-15-Ru as discussed before. *denotes spinning side-bands.

Graphical Abstract for Table of Content

Metathesis and SBA-15. The influence of pore surface functionalities in mesoporous SBA-15 silica on the stability of a model olefin metathesis catalyst, Grubbs I, is substantiated. Large portions of chemisorbed species arise from interactions between the tricyclohexylphosphine and silanols. Surface silanols significantly decreases the longevity of the ring-closing metathesis catalyst, whereas passivation of the surface slows down the catalysis rate, but does not affect significantly the lifetime of the catalyst.

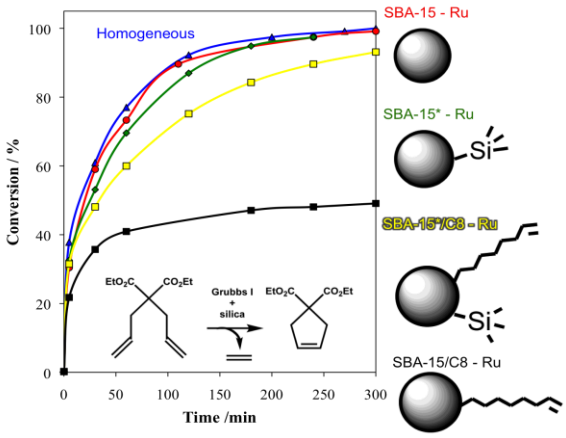

Surface organometallic chemistry

H. Staub, R. Guillet-Nicolas, N. Even, L. Kayser, F. Kleitz, F.-G. Fontaine**

Substantiating the Influence of Pore Surface Functionalities on the Stability of Grubbs Catalyst in Mesoporous SBA-15 Silica